

Supporting Information

Star-Polymer Multidentate-Cross-Linking Strategy for Superior Operational Stability of Inverted Perovskite Solar Cells at High Efficiency

Qi Cao,^a Jiabao Yang,^a Tong Wang,^a Yuke Li,^b Xingyu Pu,^a Junsong Zhao,^a Yixin Zhang,^a Hui Zhou,^a Xiaoqiang Li,^a and Xuanhua Li^{a*}

a. State Key Laboratory of Solidification Processing, Center for Nano Energy Materials, School of Materials Science and Engineering, Northwestern Polytechnical University, Xi'an, 710072, China.

b. Department of Chemistry and Centre for Scientific Modeling and Computation, Chinese University of Hong Kong, Shatin, Hong Kong, China.

* E-mail: lixh32@nwpu.edu.cn

Experimental Procedures

Materials: Nickel nitrate hexahydrate ($\text{Ni}(\text{NO}_3)_2 \cdot 6\text{H}_2\text{O}$, 99.999%), chlorobenzene (CB, 99.8%), anhydrous dimethyl sulfoxide (DMSO, 99.8%), and N,N-dimethylformamide (DMF, 99.8%) were purchased from Sigma-Aldrich. All photovoltaic materials were purchased from Xi'an Polymer Light Technology Corp. and did not require further purification. 3-Chloropropyltrimethoxysilane, pentamethyldiethylenetriamine (PMDETA), methyl methacrylate (MMA), polymethyl methacrylate (PMMA, weight-average molecular weight ($M_w \approx 6.8 \times 10^4$)), trimethylolpropane trimethacrylate (TMPTMA), pentaerythritol tetraacrylate (PT), triacetyl- β -cyclodextrin (TC), acrylonitrile, and copper(I) chloride (CuCl) was purchased from Aladdin.

Materials synthesis: The synthesis process of the POSP polymer ($M_w \approx 5.4 \times 10^5$) was divided to two steps. ① Synthesis of octa (γ -chloropropyl) silsesquioxane ($\text{POSS}-(\text{Cl})_8$): concentrated hydrochloric acid (8 mL), 3-chloropropyltrimethoxysilane (10 mL), and methanol (200 mL) were added to a 500 mL round-bottomed flask and then quickly stirred for 5 days in a 40 °C oil bath to complete the hydrolysis. The product was washed multiple times with methanol and dried under vacuum to gain white powder. ② Synthesis of the POSP polymer: the synthesis procedures were carried out using $\text{POSS}-(\text{Cl})_8$ as radical initiator in a one-pot two-step atom transfer radical polymerization. In this process, the flask was continuously flowed with dry N_2 to get rid of O_2 . Then, $\text{POSS}-(\text{Cl})_8$ (0.20 g), toluene (20 mL), MMA (20 mL), PMDETA (0.12 mL), and CuCl (0.02 g) were mixed in the flask. The flask put into an oil bath equipped with magnetic stirring bar at 110 °C. After 48 h, the flask was cooled in ice water to terminate the polymerization reaction. The mixture was then poured into tetrahydro-furan for dilution, filtered through alumina column to get rid of the catalyst and then poured into tenfold methanol-water mixed solvent. After being filtered and dried under reduced pressure at 40 °C for 24 h, the final product POSP polymer was obtained. The synthesis of this polymer is simple and it can be prepared on a large scale.

In order to produce excellent yields and reduce the post-processing, a one-pot two-step reaction was employed to synthesize polyhedral oligomeric silsesquioxane-poly (methyl methacrylate)-b-poly (acrylonitrile) (POSPP). The polymerization processes are similar as POSP. The difference is that, after the first 24h reaction, the same volume of second monomer (acrylonitrile) was added into system and reacted for one more 24 h. The remaining purification method and the afterwards treatment were the same.

Nickel oxide nanoparticles (NiO_x NPs) were synthesized according to a previous literature¹. The CsFAMA triple-cation perovskite precursor solution was prepared by mixing lead iodide (PbI_2 , 1.30 M), cesium iodide (CsI, 0.07 M), lead bromide (PbBr_2 , 0.21 M), methylammonium bromide (MABr, 0.21 M),

and formamidinium iodide (FAI, 1.19 M) in a mixed anhydrous solvent of DMF/DMSO (4/1, V/V) and was stirred overnight.

Inverted Solar Cell Fabrication (p-i-n): ITO glasses were continuously washed in an ultrasonic bath for 15 min in detergent-deionized water solution, acetone and ethanol, respectively. The ITO glasses were dried with N₂ and then treated with UV-ozone for 15 min to increase hydrophilicity. NiO_x (20 mg ml⁻¹ in H₂O) was deposited on ITO at 4000 rpm for 30 s and then heated at 100 °C for 10 min. The thickness of the NiO_x film was approximately 20 nm. The coated ITO was then moved to a glove box. The perovskite solution was spin coated on the NiO_x hole transport layer (HTL) according to procedure that was increased from 2000 rpm for 10 s to 6000 rpm for 30 s, dropping 110 μL of the POSP polymer with various concentrations of CB antisolvent for 15 s before the end of the procedure. Then heated at 100 °C for 20 min to obtain the bright perovskite film with a thickness of 750 nm. After that, PCBM (99% purity) and Fullerene (C60, 99.5% purity) as electron transport layer (ETL) was spin-coated on the perovskite film at 3000 rpm for 30 s. The thickness of the ETL is approximately 45 nm. Next, BCP (99% purity) was spin coated on it at 6000 rpm for 30 s. Finally, fabrication of the devices was accomplished by thermally evaporating chromium (Cr, 5 nm) and gold (Au, 100 nm) electrodes under a vacuum of 2 x 10⁻⁶ mbar (0.1 cm² effective area).

Solar Cell Characterization: The SEM images of perovskite films and cross-sectional devices were obtained using FEI Helios G4 CX. TEM images were obtained with a FEI Talos F200X operating on 200 kV electron gun. XRD patterns of the perovskite films were gained by using Co target of a Bruker D8 DISCOVER A25. XPS measurements were obtained on a Kratos Axis Supra. The UPS of the perovskite films were gained by a Shimadzu Kratos photoelectron spectrometer with a non-monochromatic He I α photon source ($h\nu = 21.22$ eV). The J - V curves of PSCs were recorded under AM 1.5 G (100 mW cm⁻²) solar illumination from a Newport solar simulator, and the scan rate corresponding to the curve was 0.05 V s⁻¹. EQE spectra of the PSCs were obtained from QE-R3011 (Enli Tech) using Czerny-Turner monochromatic incident light. The steady-state PL and time-resolved PL spectra were gained by the Edinburgh Instruments FLS980 fluorescence spectrometer with 510 nm pulse excitation source wavelength. The absorption of thin films was gained using a Perkin-Elmer Lambda 35 UV-vis spectrophotometer. Mott-Schottky analysis was carried out on an electrochemical workstation (Chenhua 760) and was measured in the 0-1.5 V voltage range and 1000 Hz frequency under dark. FT-IR spectra were measured on a Jasco FT-IR-6100 in a wavelength range of 4000 to 650 cm⁻¹. ¹H-NMR measurements were obtained by a Bruker AVANCF-300 instrument with tetramethylsilane (TMS) as an internal reference. TGA was obtained by a METTLER TGA/DSC 3+. The change of light absorption during spin-coating of perovskite film was studied by self-made in-situ light absorption device.² The ToF-

SIMS was measured by a ToF-SIMS 5-100 instrument (ION-TOF GmbH, Germany). The depth profiling was obtained through a 2 keV Cs sputtering beam raster of 300×300 μm area. DLS (Dynamic Light Scattering) data were measured by Malvern zetasizer nano.

Stability test: The complete PSCs could be encapsulated in a N₂ glove box with a cover glass and UV adhesive (LT-U001, Lumtec). The operational stability of the encapsulated cells was measured at 45 °C under a white light emitting diode lamp with sixteen-channel thin film photovoltaic maximum power point tracking test system (YH-VMPP-16).

Results and Discussion

Supplementary Note 1

Admittance spectroscopy (AS) and Mott–Schottky analysis³

To reveal the passivation effect of the POSP polymer more directly and clearly, the admittance spectroscopy (AS) was conducted on the devices without and with the POSP polymer. AS is an effective technique for estimating both the energy level of trap states and the distribution of trap state density, which has been extensively applied to many photovoltaic systems, such as organic solar cells, Cu₂ZnSnS₄ solar cells, and PSCs. As the literature reported, for a p-type perovskite semiconductor, the defect activation energy (E_a) is approximately the depth of the trap state energy level (E_T) relative to the valence band maximum (VBM) energy level (E_{VBM}) of perovskite ($E_a = E_T - E_{VBM}$). E_a and the characteristic

transition angular frequency (ω_0) can be expressed in the relation $\omega_0 = \beta T^2 \exp\left(-\frac{E_a}{k_B T}\right)$, where β is a temperature dependent parameter, T is the temperature and k_B is the Boltzmann's constant. The ω_0 is determined by the derivative of the capacitance–frequency spectrum. According to this equation, the

Arrhenius plot ($\ln\left(\frac{\omega_0}{T^2}\right) = \ln \beta - \frac{E_a}{k_B T}$), and the value of E_a can be obtained from the slope of the Arrhenius

plot line. The distribution of trap state density can be derived from the equation, $N_T(E_\omega) = -\frac{V_{bi} dC}{qWd\omega k_B T}$,

$E_\omega = k_B T \ln\left(\frac{\omega_0}{\omega}\right)$, where V_{bi} is the built-in potential, W is the depletion width, q is the elementary charge, C is the capacitance, and ω is the applied angular frequency. V_{bi} and W can be extracted from the Mott–Schottky analysis through the capacitance–voltage measurement. According to the depletion

approximation, the C , V_{bi} , and W at the junction can be expressed in the relation, $\frac{C}{A} = \frac{\epsilon \epsilon_0 N}{W} = \sqrt{\frac{q \epsilon \epsilon_0 N}{2(V_{bi} - V)}}$,

where A is active area, ϵ is the static permittivity of perovskite, ϵ_0 is the permittivity of free space, N is the apparent doping profile in the depleted layer, and V is the applied bias. A Mott-Schottky plot ($\frac{A^2}{C^2} = \frac{2(V_{bi} - V)}{q \epsilon \epsilon_0 N}$) describes a straight line where the intersection on the bias axis determines V_{bi} and the slope

gives the impurity doping density N . Then, the depletion width $W = \sqrt{\frac{2 \epsilon \epsilon_0 V_{bi}}{qN}}$ corresponding to the zero bias can be calculated.

Computational details

All the calculations were performed using the Gaussian 09 programs. All of the structures were fully optimized with the B3LYP^{4, 5} method and Ahlrichs' split-valence def2-SVP basis set.⁶ Grimmes's DFT-D3 dispersion correction was used to describe the van der waals interaction.⁷

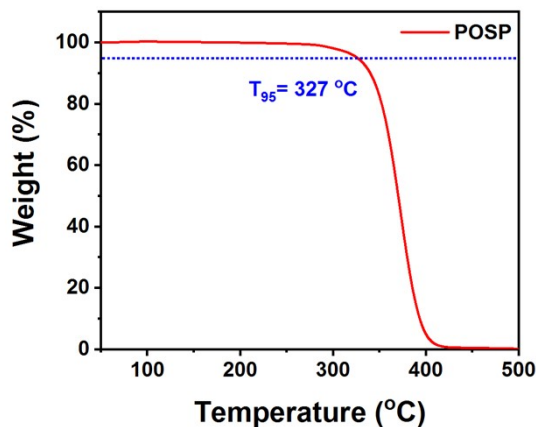


Figure S1. Thermogravimetric analysis (TGA) curves of the POSP polymer.

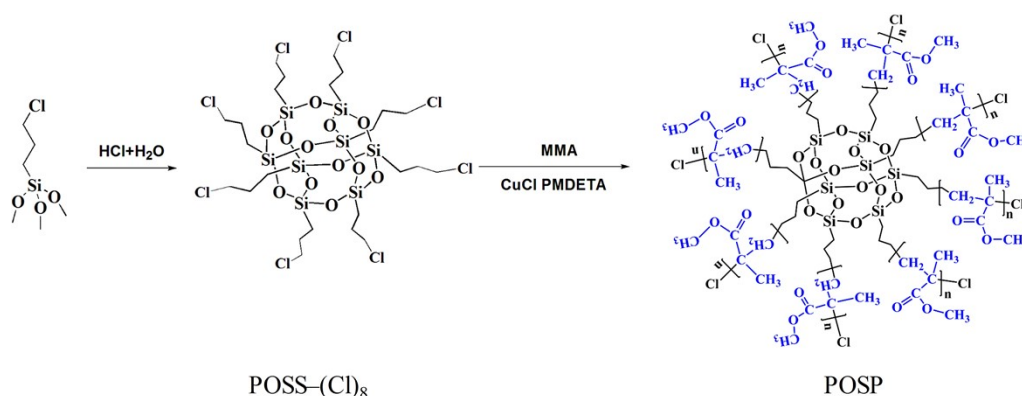


Figure S2. Synthesis route of star-shaped POSP polymer.

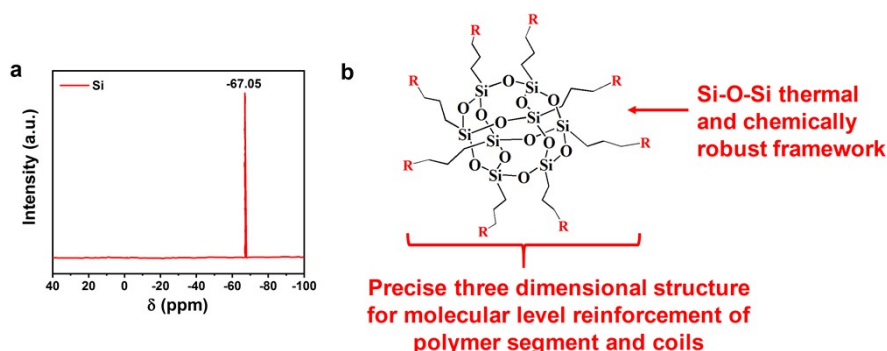


Figure S3. (a) ²⁹Si NMR of POSP. (b) POSS-R features.

There is only one single resonance at -67.05 ppm in the ²⁹Si spectrum, which indicates that the eight silicon atoms are magnetically equivalent. The resonance that appears in the range -50 ppm to -80 ppm is assigned to the chemical environment of T-type silanol silicon, which confirms that each silicon atom connects with three oxygen atoms and one carbon atom (Figure S2a). Therefore, the equivalent of eight

silicon atoms and the T-shaped silanol silicon structure prove that the core of POSP has a three-dimensional symmetrical siloxane cubic-octameric cage framework (Figure S2b).

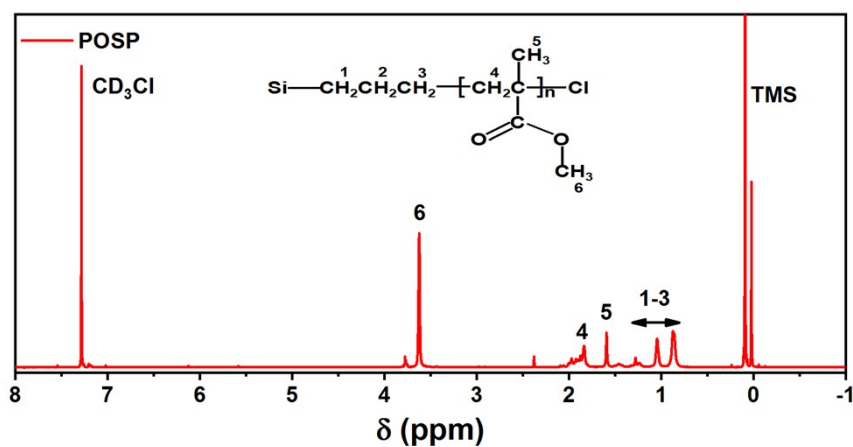


Figure S4. $^1\text{H-NMR}$ spectroscopy of the POSP polymer. Tetramethylsilane (TMS) as an internal reference, and chloroform- d_3 (CDCl_3) as solvent.

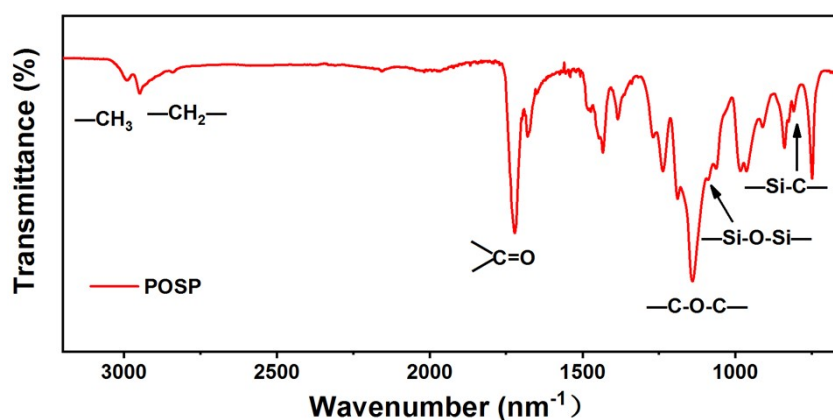


Figure S5. FT-IR spectrum of the POSP polymer.

The FT-IR spectrum shows the appearances of peaks at 1086, 1722, 2948, and 2991 cm^{-1} which are consistent with stretching vibration of Si-O-Si , $\text{C}=\text{O}$, $-\text{CH}_2$, and $-\text{CH}_3$ on chain. The absorption peaks of C-O-C and Si-C stretching vibration are observed at 1140 cm^{-1} and 805 cm^{-1} , respectively.

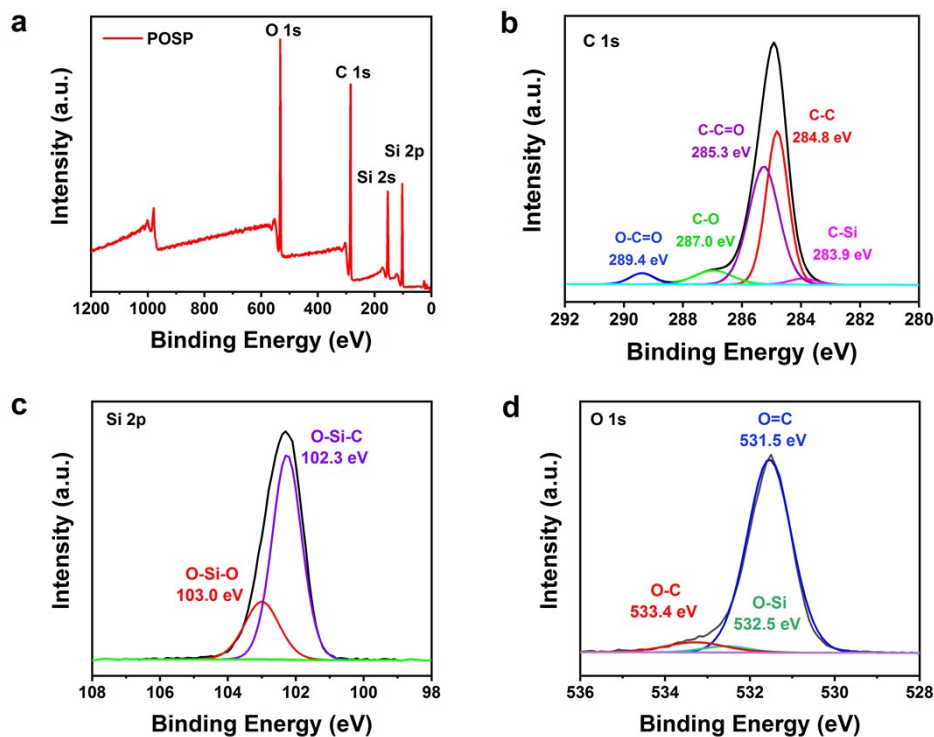


Fig. S6. (a) XPS full spectra of the POSP polymer. XPS spectra of (b) C 1s, (c) Si 2p, and (d) O 1s for the POSP polymer.

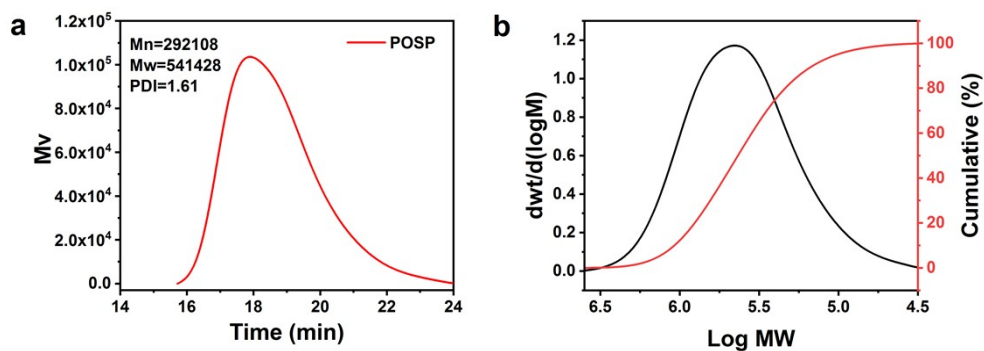


Figure S7. (a) Mass-average molecular weight (M_w), and (b) Peak molecular weight (M_p) of the POSP polymer measured by GPC.

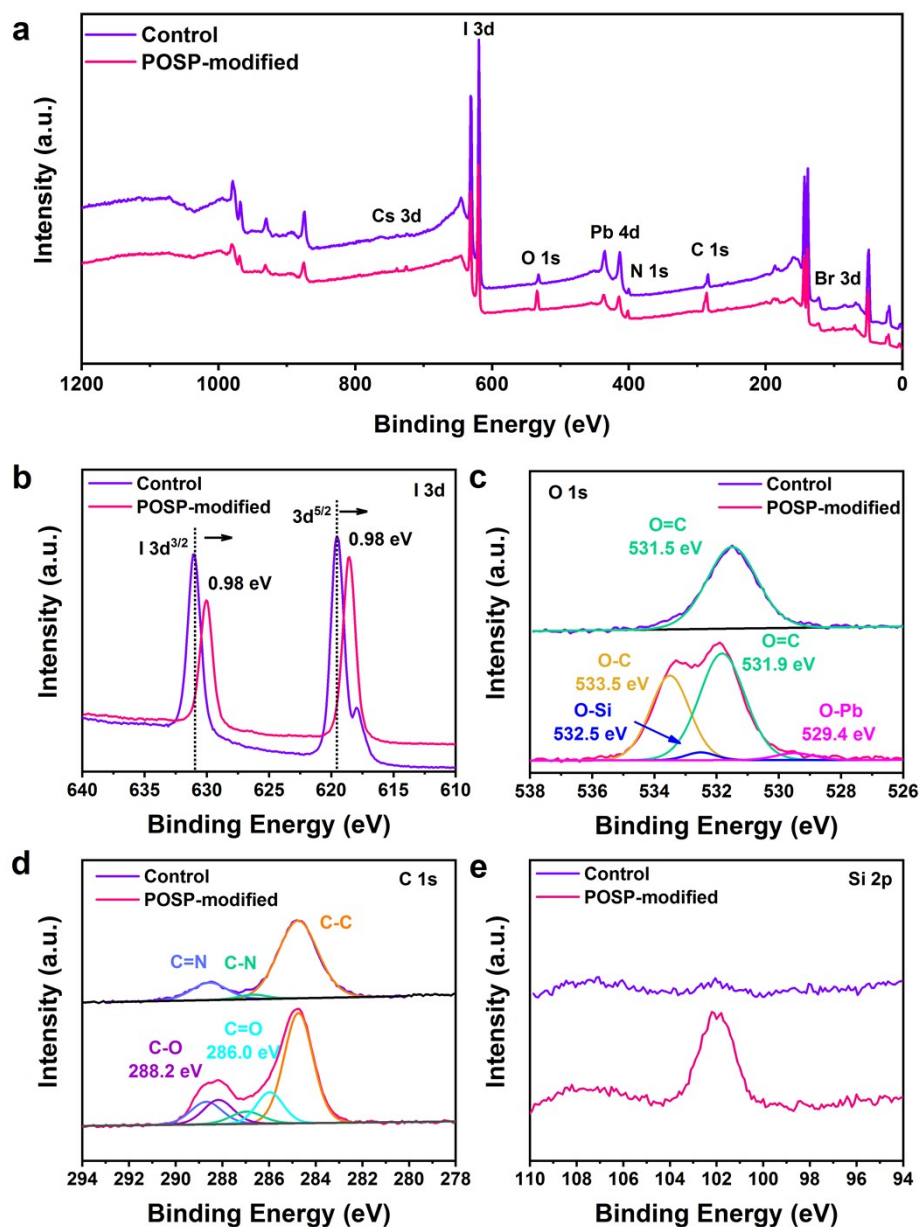


Figure S8. (a) XPS full spectra of the control and POSP-modified perovskite films. XPS spectra of (b) I 3d, (c) O 1s, (d) C 1s, and (e) Si 2p for the control and POSP-modified perovskite films.

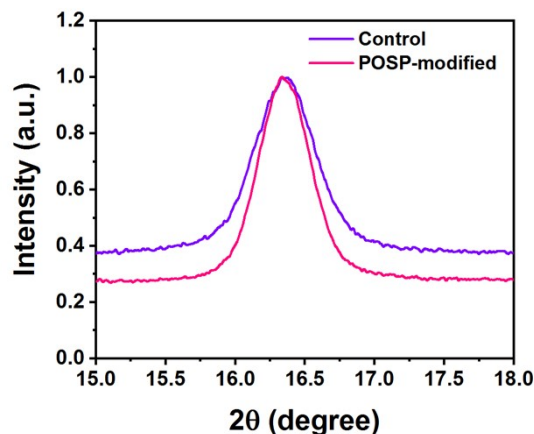


Figure S9. The full width at half maximum (FWHM) of the (100) peak intensity plane of the control and POSP-modified perovskite films.

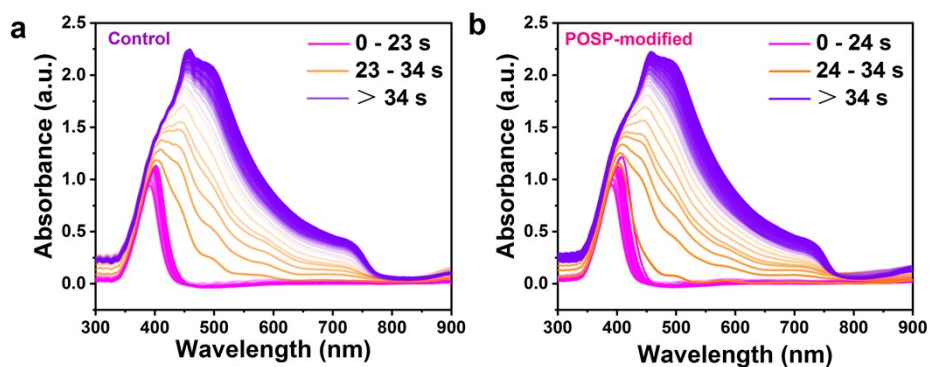


Figure S10. The in-situ absorption spectra during spinning processes for the (a) control and (b) POSP-modified films.

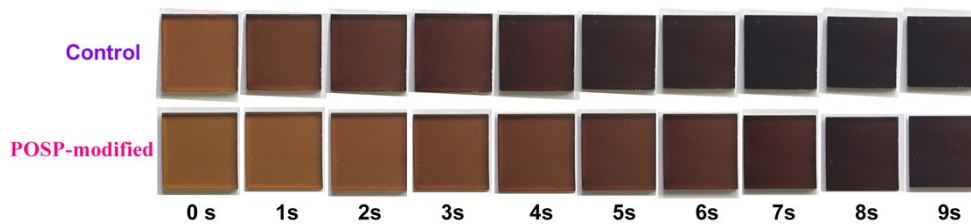


Figure S11. Photographs of color evolution of control and POSP-modified films as a function of annealing time.

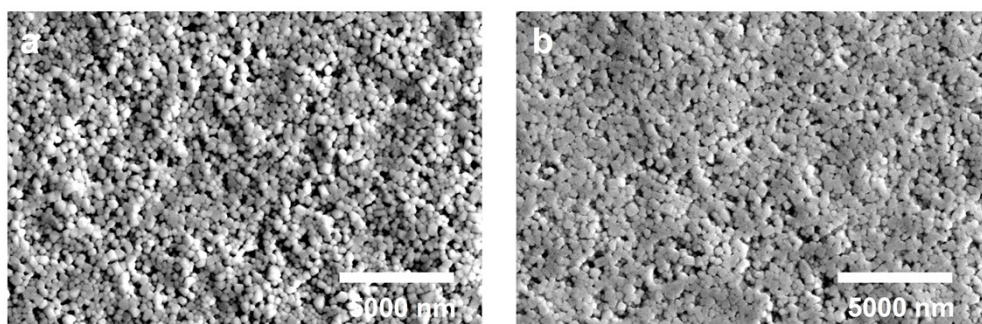


Figure S12. Top-view SEM images of the (a) control and (b) POSP-modified perovskite films (before annealing).

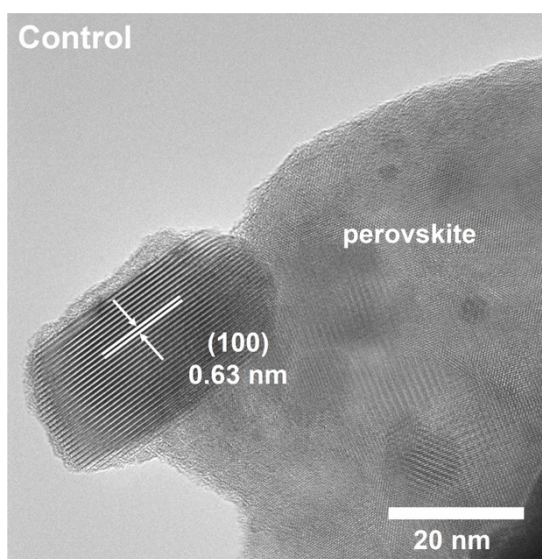


Figure S13. TEM image of the control perovskite grains.

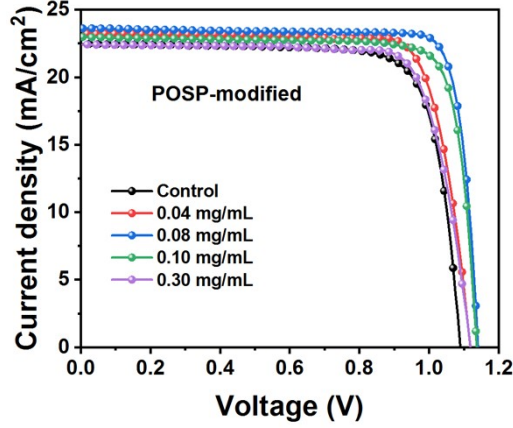


Figure S14. Optimum J - V curves of the PSCs with different POSP polymer concentration (mg mL^{-1}) in the reverse scan direction.

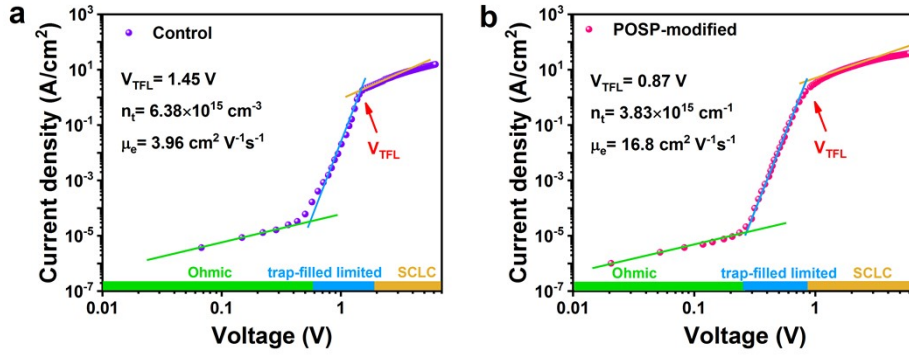


Figure S15. J - V curves of the electron-only (ITO /SnO₂/(a) control or (b) POSP-modified /PCBM /Ag).

The trap state density is determined by trap-filled limited voltage (V_{TFL}) and derived from the following equation:

$$V_{TFL} = \frac{en_t L^2}{2\epsilon\epsilon_0} \quad (1)$$

where e is the electron charge, n_t is trap state density, L is the thickness of perovskite film, ϵ is the relative dielectric constant of perovskite ($\epsilon=25.5$), and ϵ_0 is the vacuum permittivity.

The mobility is obtained according to the space charge limit current (SCLC) regions ($n=2$), the dark current was fitted by the Mott-Gurney law:

$$J = \frac{9}{8} \epsilon\epsilon_0 \mu \frac{V^2}{L^3} \quad (2)$$

where J , μ , and V are the dark current, the mobility of control or POSP-modified film, and applied voltage, respectively.

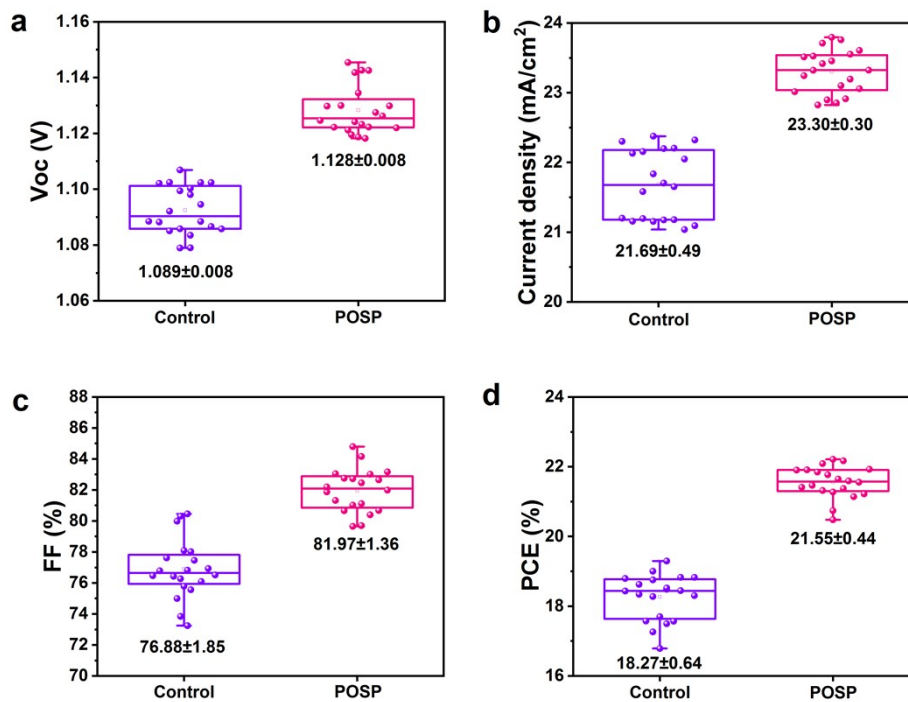


Figure S16. (a) V_{oc} , (b) J_{sc} , (c) FF, and (d) PCE statistics of 20 devices for the control and POSP-modified PSCs.

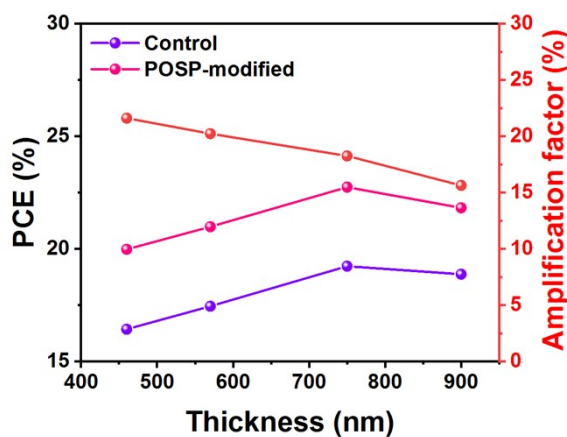


Figure S17. The relationship between the thickness of the perovskite film and the efficiency of the control and POSP-modified devices and the change of the amplification factor.

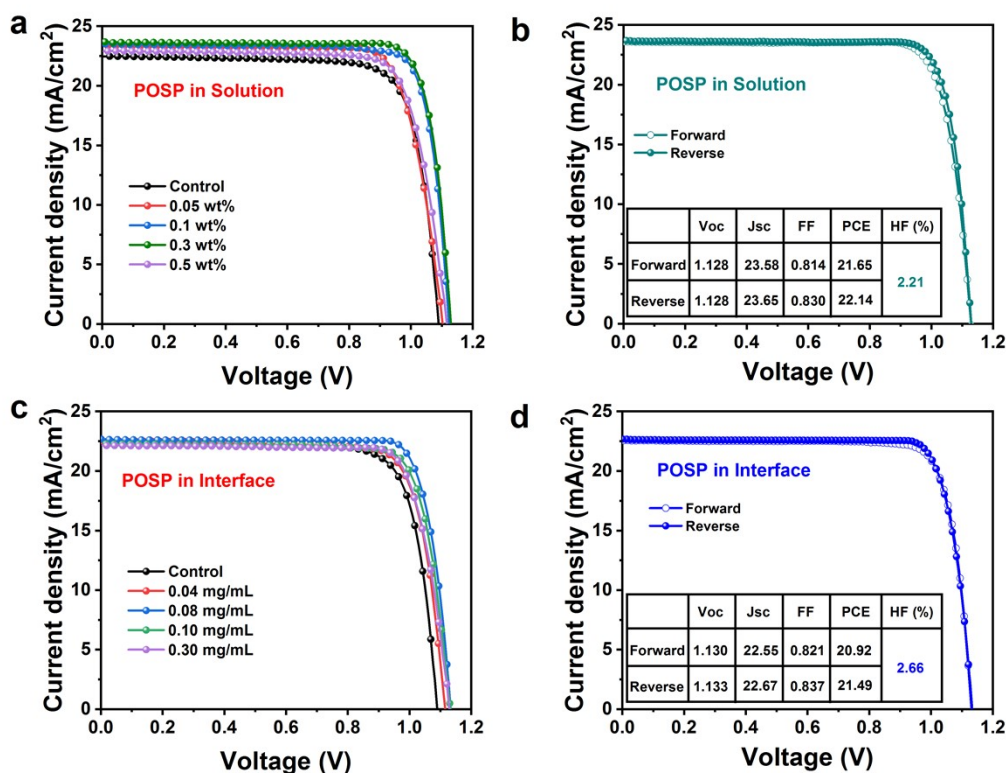


Figure S18. (a) Optimum J - V curves of the PSCs with different POSP polymer additive concentration (wt%) in the reverse scan direction. (b) J - V characteristics of the champion POSP-modified PSCs. (c) Optimum J - V curves of the PSCs with different POSP polymer interface treatment concentration (mg mL⁻¹) in the reverse scan direction. (d) J - V characteristics of the champion PSCs handled by the POSP interface.

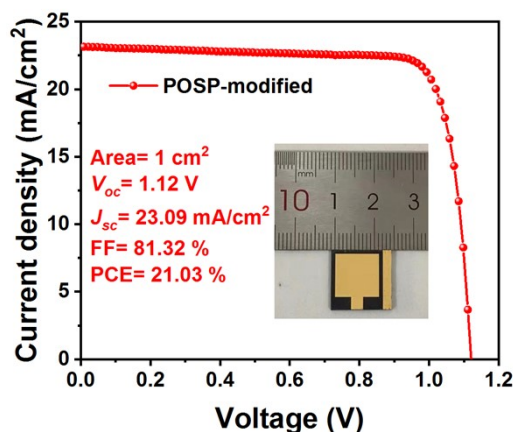


Figure S19. J - V curve of the optimal POSP-modified PSCs of area 1 cm².

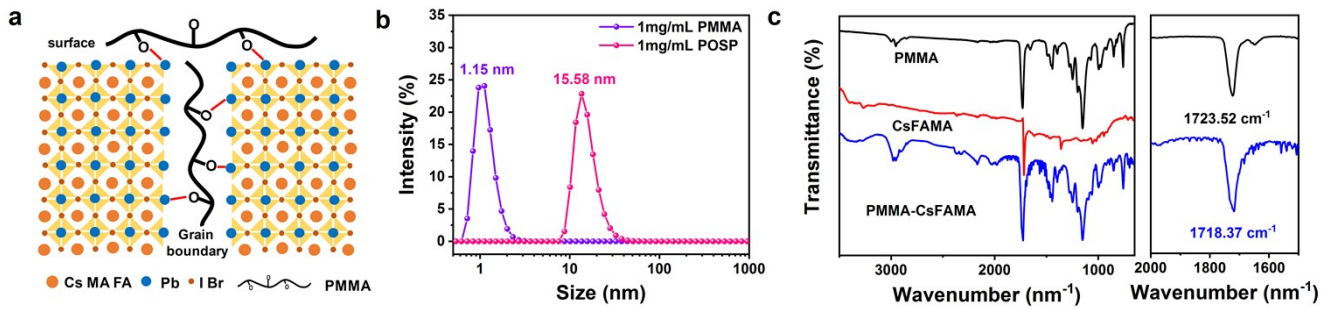


Figure S20. (a) Schematic diagram of the chelation interaction between C=O in the PMMA polymer and Pb in perovskite. (b) DLS data of PMMA and POSP polymer dissolved in chlorobenzene. (c) FTIR spectra of the PMMA polymer, CsFAMA, and PMMA-CsFAMA.

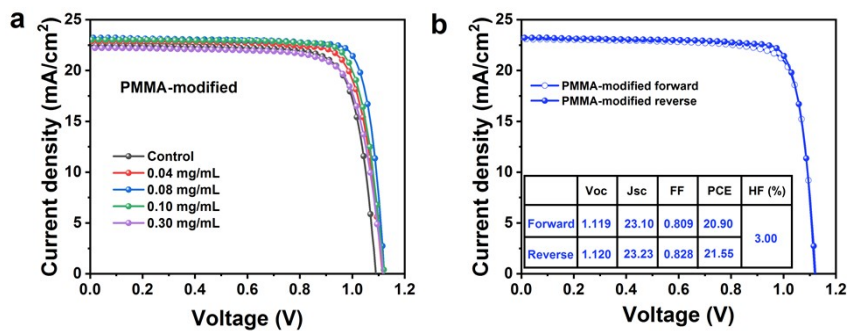


Figure S21. (a) Optimum J - V curves of the PSCs with different PMMA polymer concentration (mg mL⁻¹) in the reverse scan direction. (b) Champion J - V curves obtained in forward and reverse scans of the PMMA-modified PSCs.

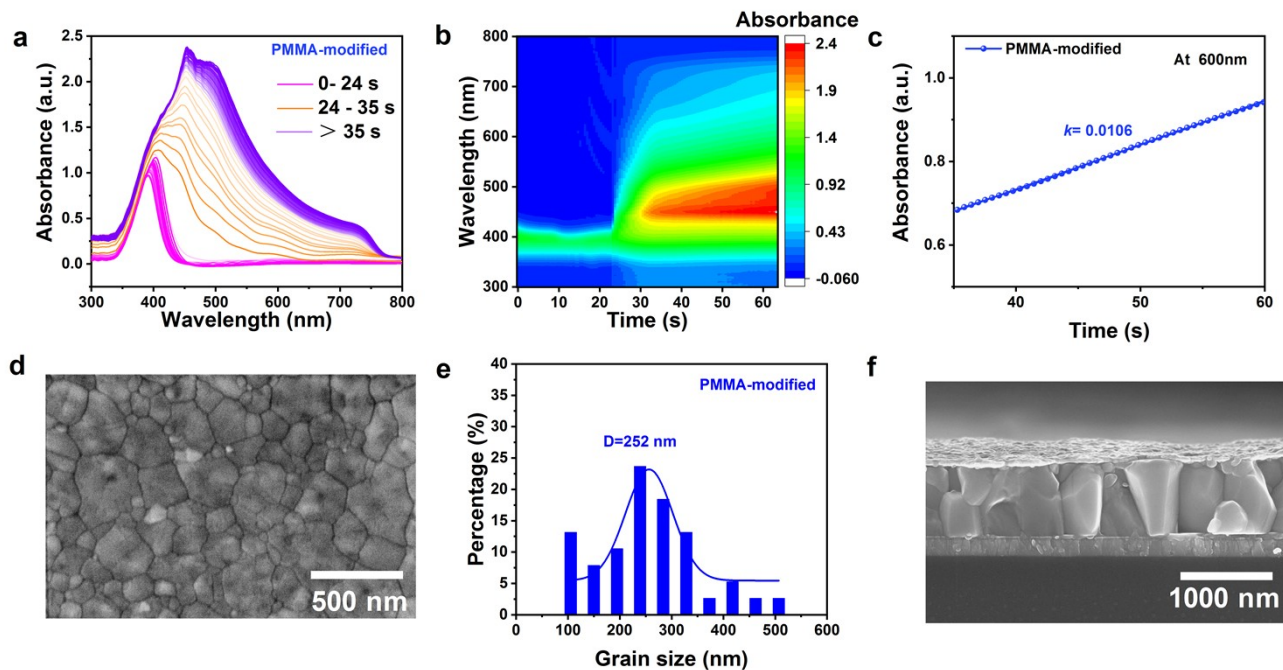


Figure S22. (a-b) The in-situ absorption spectra during spinning processes for the PMMA-modified films. (c) UV-vis absorbance at 600 nm of the PMMA-modified perovskite film as a function of spinning time in air. (d) Top-view SEM images of the PMMA-modified perovskite film. (e) Histogram of grain size distribution corresponding to the top-view SEM of the PMMA-modified perovskite film. (D represents the average grain size). (f) Cross-sectional SEM images of the PMMA-modified device (Au/perovskite/ITO).

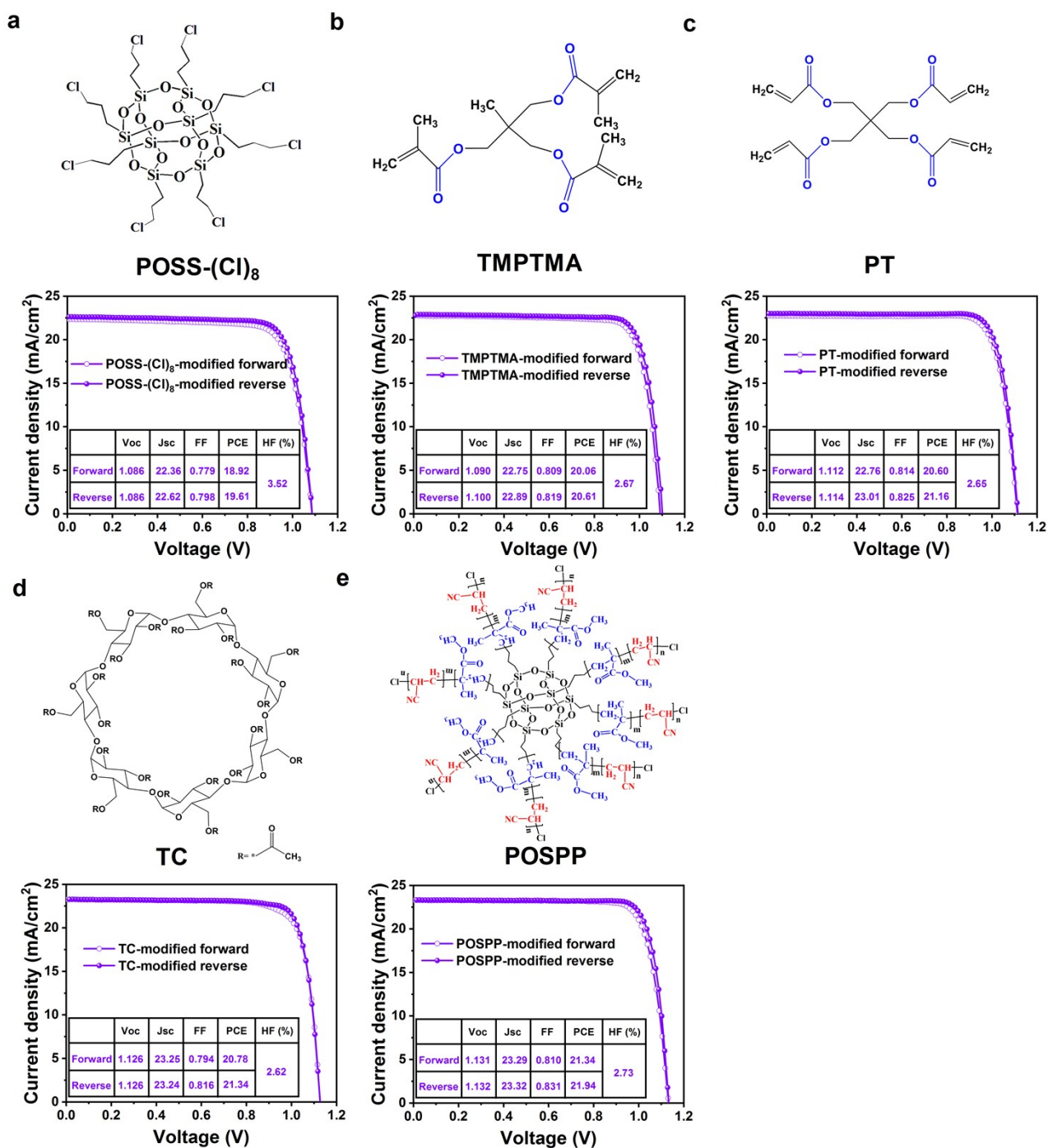


Figure S23. (a) Octa (γ -chloropropyl)-polyhedral oligomeric silsesquioxane (POSS-(Cl)₈), (b) Trimethylolpropane trimethacrylate (TMPTMA), (c) Pentaerythritol Tetraacrylate (PT), (d) Triacetyl- β -cyclodextrin (TC), and (e) Polyhedral oligomeric silsesquioxane-poly (methyl methacrylate)-b-poly (acrylonitrile) (POSPP) modify PSCs by anti-solvent method and the corresponding J - V curves.

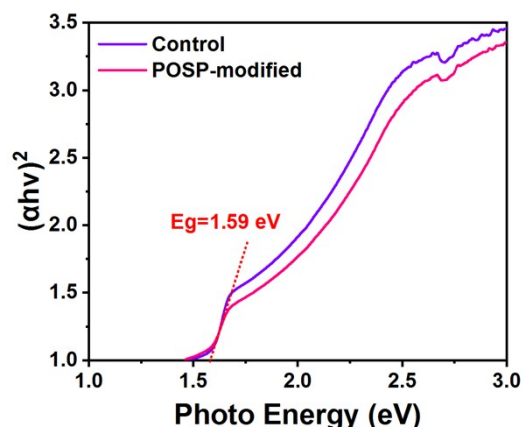


Figure S24. Tauc plots of the control and POSP-modified films.

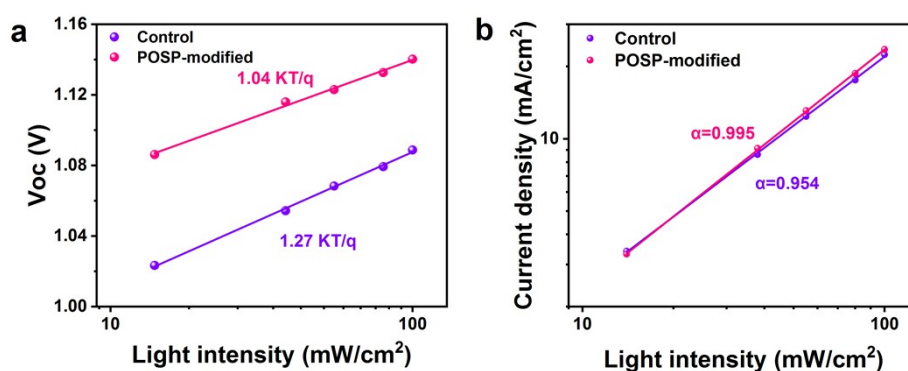


Figure S25. (a) V_{oc} and (b) J_{sc} dependent on various illumination intensities.

The carrier recombination mechanism is further attained via the current and voltage dependence on incident light intensity for the control and POSP-modified device (Figure S15). The slope of kT/q unit determines whether the trap-induced non-radiative recombination is predominated in the fabrication PSCs (where k is the Boltzmann constant, T is thermodynamic temperature, and q is the electron charge). The slope of V_{oc} versus log-scaled light-intensity reduces from $1.27 kT/q$ (control) to $1.04 kT/q$ (POSP-modified), suggesting a reduction of trap-induced recombination under open circuit conditions. According to the power law $J_{sc} \propto I^\alpha$ (where α is an exponential factor), the dependence of J_{sc} on the light intensity can be identified. The respectively calculated α values are 0.954 and 0.995 for control and POSP-modified PSCs, illustrating the decrease of bimolecular recombination under short circuit conditions. These results indicate that the effective defect passivation of perovskite treated with the 3D POSP polymer with multiple chemical anchor sites can suppress charge carrier recombination, which is beneficial to the development of device performance.

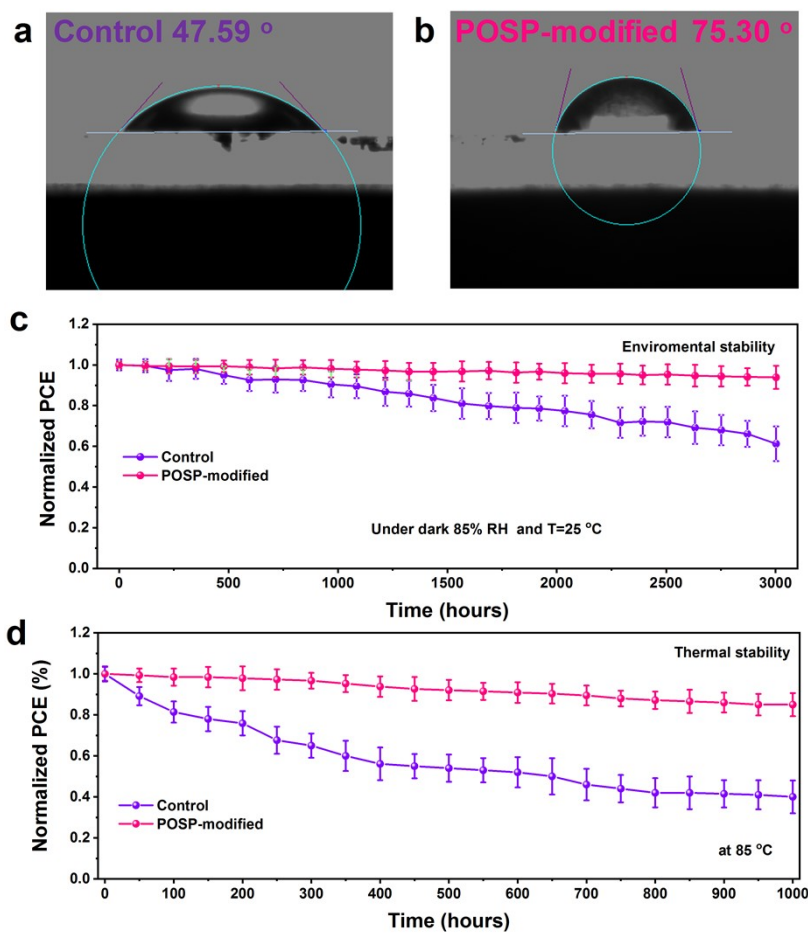


Figure S26. The contact angle of the (a) control and (b) POSP-modified perovskite films. (c) Environmental stability for the unencapsulated control and PPP-modified devices (the average PCE is obtained from 10 devices of each type of device, and the error bars represent the standard deviations of the devices). (d) Devices thermal stability upon 85 °C continuous annealing in nitrogen box.

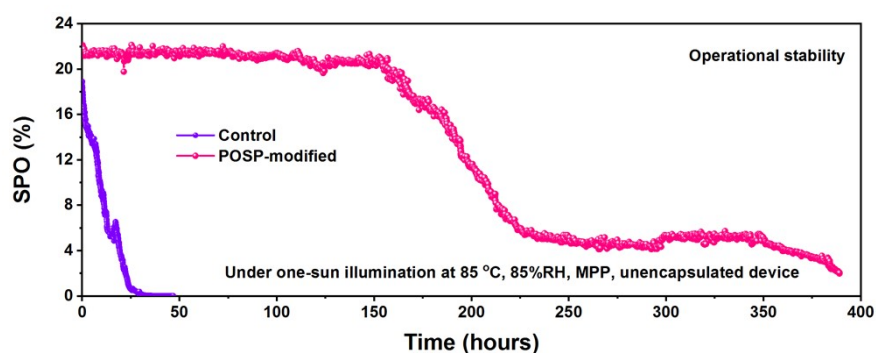


Figure S27. Evolution of SPOs of unencapsulated control and POSP-modified perovskite solar cells aged under one-sun illumination at double 85 aging conditions.

Table S1. The fitting parameters for time-resolved PL of the control and POSP-modified perovskite films.

Sample	τ_1 [ns]	A_1 [%]	τ_2 [ns]	A_2 [%]	τ_{avg} [ns]
Control	130	53.33	590	46.67	498
POSP-modified	300	27.59	1270	72.41	1190

$$\tau_{avg} = \frac{A_1\tau_1^2 + A_2\tau_2^2}{A_1\tau_1 + A_2\tau_2} \quad (3)$$

Fit the time-resolved PL decay curves to a biexponential decay function:

$$Y = A_1 \exp\left(-\frac{t}{\tau_1}\right) + A_2 \exp\left(-\frac{t}{\tau_2}\right) + y_0 \quad (4)$$

where A_1 and A_2 represent the relative amplitude, τ_1 and τ_2 represent the fast and slow decay lifetimes, severally.

Table S2. The best photovoltaic parameters of inverted PSCs for the control and POSP-modified device with different POSP concentration measured in reverse scan directions under standard AM 1.5 illumination (100 mW cm^{-2}).

	Concentration [mg mL^{-1}]	V_{oc} [V]	J_{sc} [mA cm^{-2}]	FF	PCE [%]
	control (0)	1.088	22.48	0.786	19.23
anti-solvent	0.04	1.119	23.21	0.801	20.80
	0.08	1.139	23.56	0.848	22.74
	0.10	1.136	22.95	0.824	21.49
	0.30	1.119	22.42	0.786	19.74
	0.04	1.114	22.59	0.795	20.01
interface	0.08	1.133	22.67	0.837	21.49
	0.10	1.131	22.24	0.810	20.38
	0.30	1.128	22.13	0.808	20.16
	Concentration [wt%]	V_{oc} [V]	J_{sc} [mA cm^{-2}]	FF	PCE [%]
solution	0.05	1.102	23.33	0.791	20.32
	0.1	1.122	23.47	0.816	21.47
	0.3	1.128	23.65	0.830	22.14
	0.5	1.115	22.93	0.783	20.03

Table R3. The best photovoltaic parameters of inverted PSCs for the control and PMMA-modified device with different PMMA concentration measured in reverse scan directions under standard AM 1.5 illumination (100 mW cm^{-2}).

Concentration (mg mL^{-1})	V_{oc} [V]	J_{sc} [mA cm^{-2}]	FF	PCE [%]
control (0)	1.088	22.48	0.786	19.23
0.04	1.115	22.89	0.795	20.29
0.08	1.120	23.23	0.828	21.55
0.10	1.120	23.03	0.809	20.88
0.30	1.117	22.23	0.769	19.10

References

1. S. Wang, B. Yang, J. Han, Z. He, T. Li, Q. Cao, J. Yang, J. Suo, X. Li, Z. Liu, S. F. Liu, C. Tang and A. Hagfeldt, *Energy Environ. Sci.*, 2020, **13**, 5068-5079.
2. M. Zhang, T. Li, J. Yu, G. Lu, H. Zhou and X. Zhan, *Sol. RRL*, 2020, **4**, 2000140.
3. S. Ye, H. Rao, Z. Zhao, L. Zhang, H. Bao, W. Sun, Y. Li, F. Gu, J. Wang, Z. Liu, Z. Bian and C. Huang, *J. Am. Chem. Soc.*, 2017, **139**, 7504-7512.
4. G. Scalmani and M. J. Frisch, *J. Chem. Phys.*, 1993, **98**, 5648-5652.
5. C. Lee, W. Yang and R. G. Parr, *Phys. Rev. B Condens. Matter*, 1988, **37**, 785-789.
6. A. Schäfer, H. Horn and R. Ahlrichs, *J. Chem. Phys.*, 1992, **97**, 2571-2577.
7. S. Grimme, J. Antony, S. Ehrlich and H. Krieg, *J. Chem. Phys.*, 2010, **132**, 154104.